Cement and Concrete Research 161 (2022) 106961

Contents lists available at ScienceDirect

Cement and Concrete Research

journal homepage: www.elsevier.com/locate/cemconres

Effect of fineness of cement on drying shrinkage

Ippei Maruyama [a,b,*], Hiroki Sugimoto [c], Syota Umeki [a], Ryo Kurihara [b]

[a] Department of Environmental Engineering and Architecture, Graduate School of Environmental Studies, Nagoya University, Nagoya, Japan
[b] Department of Architecture, Graduate School of Engineering, The University of Tokyo, Japan
[c] Niigata Building Technology Center, East Japan Railway Company, Japan

ARTICLE INFO

Keywords:
(a) Drying
(b) Calcium-silicate-hydrate (C–S–H)
(b) Microstructure
(b) Surface area

ABSTRACT

The effect of fineness of cement on drying shrinkage was investigated. Three cement paste samples with different fineness values were prepared from the same clinker. The changes in length and mass, and water vapor sorption of the dried cement pastes after 3, 7, 28, and 91 d of curing were obtained. The relationships between drying shrinkage and the degree of hydration were not identical under the different cement fineness values. Therefore, there exists another mechanism behind the increase in drying shrinkage, apart from the faster degree of hydration. It was found that drying shrinkage is well predicted by the index $S_{H2O,v} \times B$, where B denotes the Blaine value of cement, and $S_{H2O,v}$ represents the water vapor sorption surface area. Hence, it was deduced that C–S–H undergoes an anisotropic volume change under drying and a greater shrinkage in the circumferential direction of the original cement grains.

1. Introduction

The drying shrinkage of hardened cement paste (hcp) is vital to concrete. It induces cracking around the aggregate [1–8] and these cracks reduce the Young's modulus and strength of concrete [9–18], while drying itself has an influence on strength increase of hcp [19–22]. The drying shrinkage of concrete is primarily driven by the drying shrinkage of hcp, and shrinkage-induced visible cracks in concrete members, which are yielded under the restraint condition, affect the durability of concrete [23] as well as the structural performance of concrete [24–29]. Consequently, it is important to understand, predict, and control the drying shrinkage of hcp.

The drying shrinkage mechanism is yet to be elucidated despite extensive investigations [30–38]. This might be because the hcp undergoes microstructure changes during the first drying, and the mechanism of drying shrinkage is not the same as that of rigid porous materials. Irreversible shrinkage was originally reported by Helmuth and Turk [39]; they discovered that the effect of the water-to-cement ratio on the drying shrinkage is attributable to the different irreversible shrinkage strains, which originate from the colloidal nature of calcium silicate hydrate (C–S–H) [19,40–45]. Microstructural change during the first drying, which is associated with the yielding of the irreversible strain, was confirmed in long-term drying conditions exceeding 40 % RH. Previous studies have investigated microstructural changes during the first desorption using nitrogen sorption isotherms [46–48], water vapor sorption isotherms [49], small-angle X-ray or neutron scattering [50–55], microscopy observations [24,56,57], low-temperature calorimetry [58,59], nuclear magnetic resonance on C–S–H [49,60], and ^{1}H NMR relaxometry [44,61–63].

In previous studies, two types of C–S–H in Portland cement paste were primarily investigated, namely low- and high-density C–S–H [41,64,65], and the amount of low-density C–S–H was estimated based on the nitrogen sorption Brunauer, Emmett, and Teller (BET) surface area [66]. This nitrogen BET surface area and sorption isotherms change after long-term drying [46–48], and a qualitative correlation exists between the amount of low-density C–S–H and the irreversible shrinkage strain [39,66], which appears to correspond to irreversible shrinkage.

Based on microscopy, outer C–S–H [67,68] which is the C–S–H precipitated outside of the original particle boundary of cement and in the relatively early stage of the clinker hydration process [69], contributes significantly to surface area development [65] owing to its low density and sparse structure. It is noteworthy that this outer C–S–H may become high-density C–S–H in the later stage of cement hydration; this can be regarded as the reduction in gel pore water via ^{1}H NMR relaxometry [70] or the reduction in the nitrogen BET surface area with increasing hydration degree in the hcp [66]. Therefore, the outer C–S–H does not correspond to the low-density C–S–H, whereas the low-density C–S–H is composed of the outer C–S–H.

* Corresponding author at: Department of Architecture, Graduate School of Engineering, The University of Tokyo, Japan.
E-mail address: i.maruyama@bme.arch.t.u-tokyo.ac.jp (I. Maruyama).

https://doi.org/10.1016/j.cemconres.2022.106961
Received 2 February 2022; Received in revised form 9 August 2022; Accepted 26 August 2022
Available online 6 September 2022
0008-8846/© 2022 Elsevier Ltd. All rights reserved.

Table 1
Blaine value and characteristics of particle size distribution of cements.

	Blaine	Median diameter	Mode diameter	Mean diameter
	(m^2/kg)	(μm)	(μm)	(μm)
N-LB	244	29.3	44.0	36.3
N-MB	338	20.0	31.1	25.3
N-HB	391	17.1	28.5	22.6

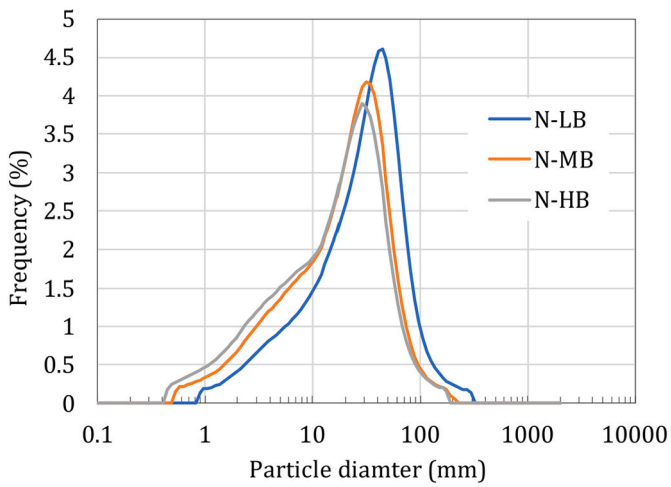

Fig. 1. Particle size distribution of cements.

Previous studies have shown that finer cement undergoes a greater drying shrinkage [68,69], which can be explained by the faster degree of hydration [71]. The higher degree of hydration of the hcp system represents a larger amount of C–S–H and a lower amount of unreacted clinker minerals. And hcp whose large portion is occupied by shrinkable materials will show a large shrinkage. However, there is no detailed research to confirm this hypothesis by measuring the degree of hydration and drying shrinkage.

Because the cement fineness is occasionally optimized (typically by increasing it) only for the construction process and strength development [72], the effect of fineness on the drying shrinkage of hcp may be vital from the perspectives of engineering and science. In this study, cement samples of three different fineness were prepared from the same clinker batch, and their hydration and shrinkage were investigated.

2. Experiment

2.1. Material

An ordinary Portland clinker was ground to prepare cement samples of three different fineness; the samples were labeled N-LB (normal cement with low Blaine value), N-MB (middle Blaine value), and N-HB (high Blaine value), based on their Blaine values. These three different Baline values were attained by changing the duration of grindings. The materials were provided by Mitsubishi Materials Corporation. The Blaine values and characteristics of the particle size distribution of each cement are summarized in Table 1. The particle size was analyzed using an image analyzer (Morphologi G2, Malvern), and the results are shown in Fig. 1. For this purpose, a well-mixed cement - 2-propanol suspension (0.5 mL) was prepared and injected onto a glass plate. After drying, the dispersed cement powder on the plate was quickly subjected to observation by Morphologi G2. Then, high-quality images of each particle were captured, and two-dimensional projection-based geometrical calculations were performed.

The chemical composition of the original clinker is shown in Table 2. The mineral composition of the clinker determined via powder X-ray diffraction (XRD) and Rietveld analysis (QXRD) is presented in Table 3.

The cement samples were mixed with deionized water at 1000 rpm using a planetary centrifugal mixer. The starting mixture proportion of the paste was 0.4, which prevented cement agglomeration avoided, and the mixing was performed for 90 s. After scrapping the cement attached to the internal capsule surface and adding the residual deionized water to achieve a cement paste with a water-to-cement ratio of 0.55, an additional 90 s of mixing was executed. Each batch of the paste was conducted at 400 cm^3, and all batches were accumulated in a stainless-steel bowl. After obtaining all the batches, the cement paste was remixed every 30 min using a spatula until the cement paste exhibited a creamy consistency similar to that in previous studies [37,49]. This occurred for approximately 8 h in order to get creamy consistency which is necessary to get homogenous specimens. Subsequently, the cement paste was cast into 3 mm × 13 mm × 300 mm slab molds, and the molds were placed in a thermostatic chamber at 20 ± 1 °C. After 3 d, they were demolded and cut into 100 mm in length and then cured in sealed conditions using aluminum coating bags.

At 3, 7, 28, and 91 d after casting, the specimens were placed under different relative humidity (RH) conditions. The RH in the chamber was controlled using a saturated saline solution. The saline types used and the corresponding RHs are summarized in Table 4.

For one RH condition of a specified drying age of a paste type, two drying chambers were prepared. One was for dummy specimens whose length and mass changes were monitored, and the other was used for the main measurement. The main measurement results were recorded after 1 year of drying.

A partial number of the main specimens dried under 11 % RH were then moved to the chambers of 33, 40, 58, 75, and 95 % RH. After 6 months, the length and mass changes of the specimens were measured.

2.2. Analysis

The length of the specimen was measured using a contact displacement meter with a precision of ±0.5 μm, and a reference specimen was

Table 3
Mineral composition of used clinker in this study.

	Alite	Belite	Aluminate	Alumino-ferrite	Periclase	Gypsum
Clinker	49.3 ± 1.8	31.2 ± 2.6	5.5 ± 0.6	11.7 ± 0.7	1.2 ± 0.3	1.1 ± 0.3

Table 4
Saturated salt solution for controlling relative humidity.

Saturated salt	$LiCl_2$	$MgCl_2$	NaI	NaBr	NaCl	KCl	KNO_3
RH (%)	11	33	40	58	75	85	95

Table 2
Chemical composition of used clinker obtained from X-ray fluorescence elemental analysis.

	L.O.I	SiO_2	Al_2O_3	Fe_2O_3	CaO	MgO	SO_3	Na_2O	K_2O	TiO_2	P_2O_5	Total
	(%)											
Clinker	0.03	21.31	5.79	3.34	65.46	1.28	1.68	0.29	0.33	0.3	0.3	100.11

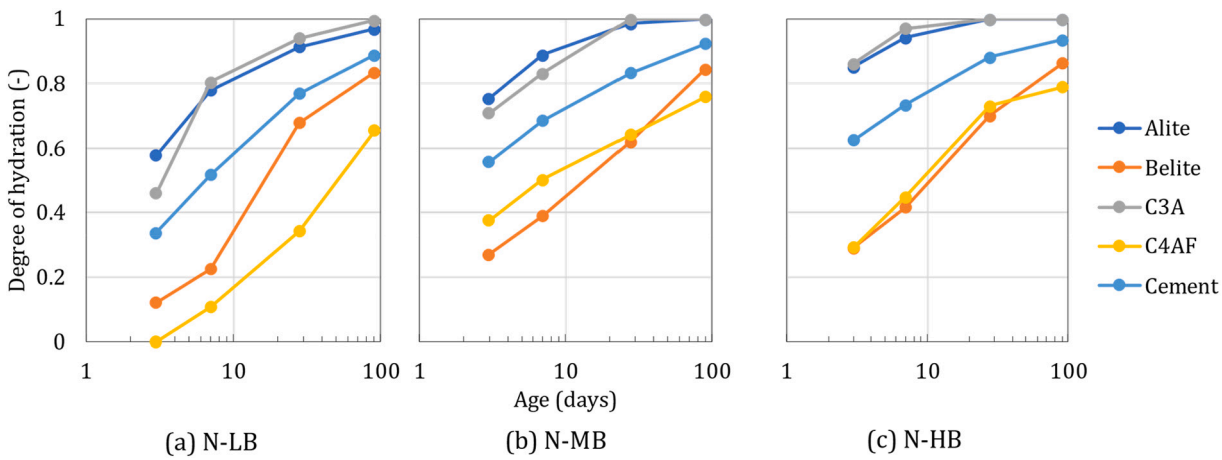

Fig. 2. Hydration degree of cement minerals and cement at start of drying.

prepared using a 100-mm-long low thermal expansion coefficient ceramic (Mitsutoyo Co.). The specimen size measurements followed those of our previous measurements [33,46,70,71]. In our previous studies [33,46,70,71,73,74], surface cracks on the surface were not confirmed. The length difference between the sample and reference ceramic was determined before and after drying in the main measurements. Only the pen-mark was used for the position of the contact displacement meter, and every measurement was conducted in the same temperature control room at 20 ± 1 °C. The mass of the specimen was measured before and after drying or heating. Five specimens were subjected to each drying condition to obtain an average value.

The phase compositions of the hcp specimens were quantified using powder XRD and QXRD. All the hcp specimens were crushed (smaller than ~1 mm blocks), submerged in isopropanol for 6 h, and then dried for several minutes using an aspirator. The crushed specimens were stored at 11 % RH and 20 ± 1 °C for 2 weeks. The specimens were ground in a ball mill, and corundum powder (10 mass%) was added to the sample powder as a standard reference. The parameters used for the XRD (D8 Advance, Bruker AXS) were as follows: tube voltage of 40 kV, tube current of 40 mA, 2θ scan range of 5°–65°, step width of 0.02°, and

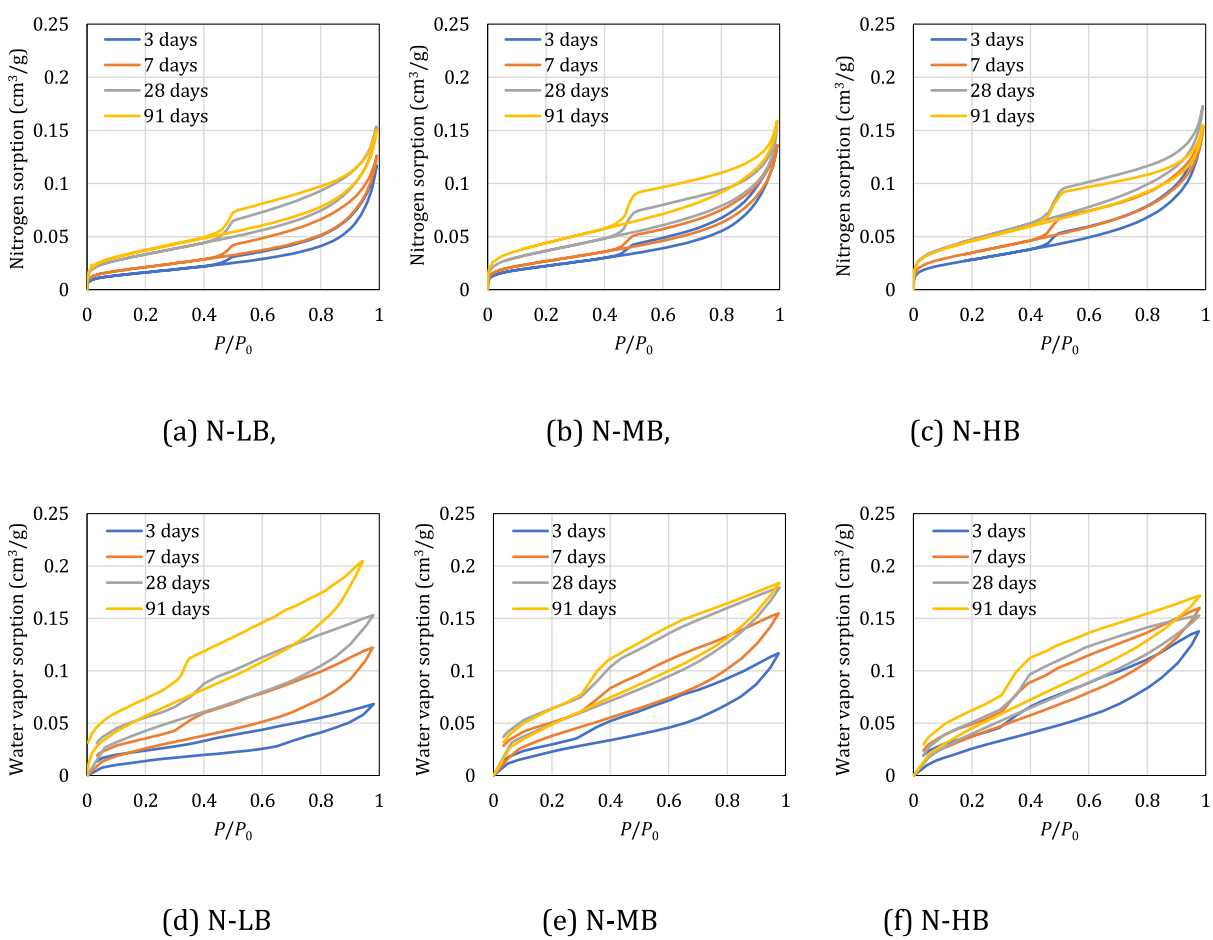

Fig. 3. Nitrogen sorption measurements for (a) N-LB, (b) N-MB, and (c) N-HB. Water vapor sorption measurements for (d) N-LB, (e) N-MB, and (f) N-HB.

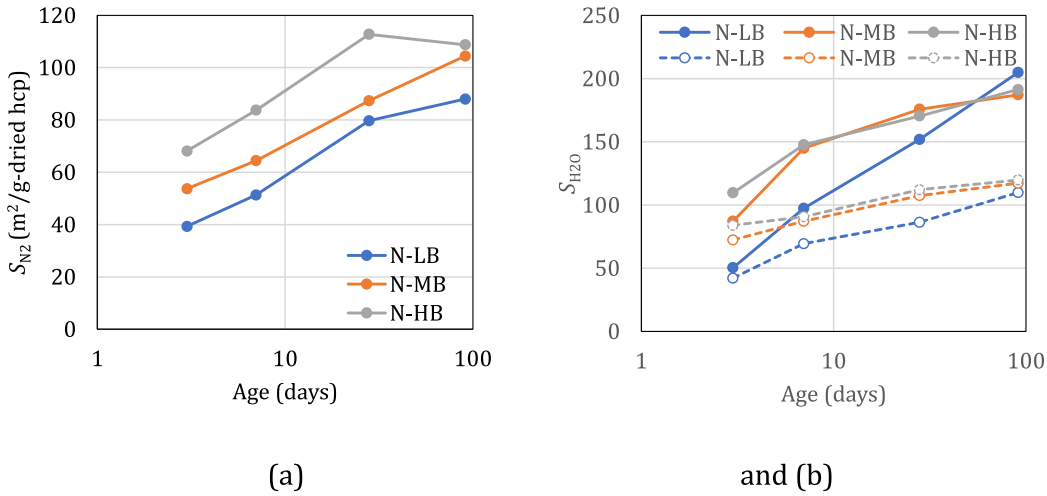

Fig. 4. (a) S_{N2} and (b) S_{H2O} of N-LM, N-MB, and N-HB as a function of time. Dotted lines in (b) represent results of specimens dried under 11 % RH for 1 year.

scan speed of 0.5°/min. The software used for the QXRD was TOPAS ver. 6.0 (Bruker AXS). The halo pattern of the amorphous phase was refined as a background function. The samples were measured thrice under each set of experimental conditions.

Thermal gravimetry (TG) was conducted. The specimen for XRD without corundum was measured from room temperature to 950 °C under nitrogen flow with 10 °C/min. Based on TG, the ratio of the mass of original cement clinker to the mass of hcp specimen was obtained. In this process, original calcite content should be corrected. Based on this ratio, degree of hydration of each clinker was calculated by using the

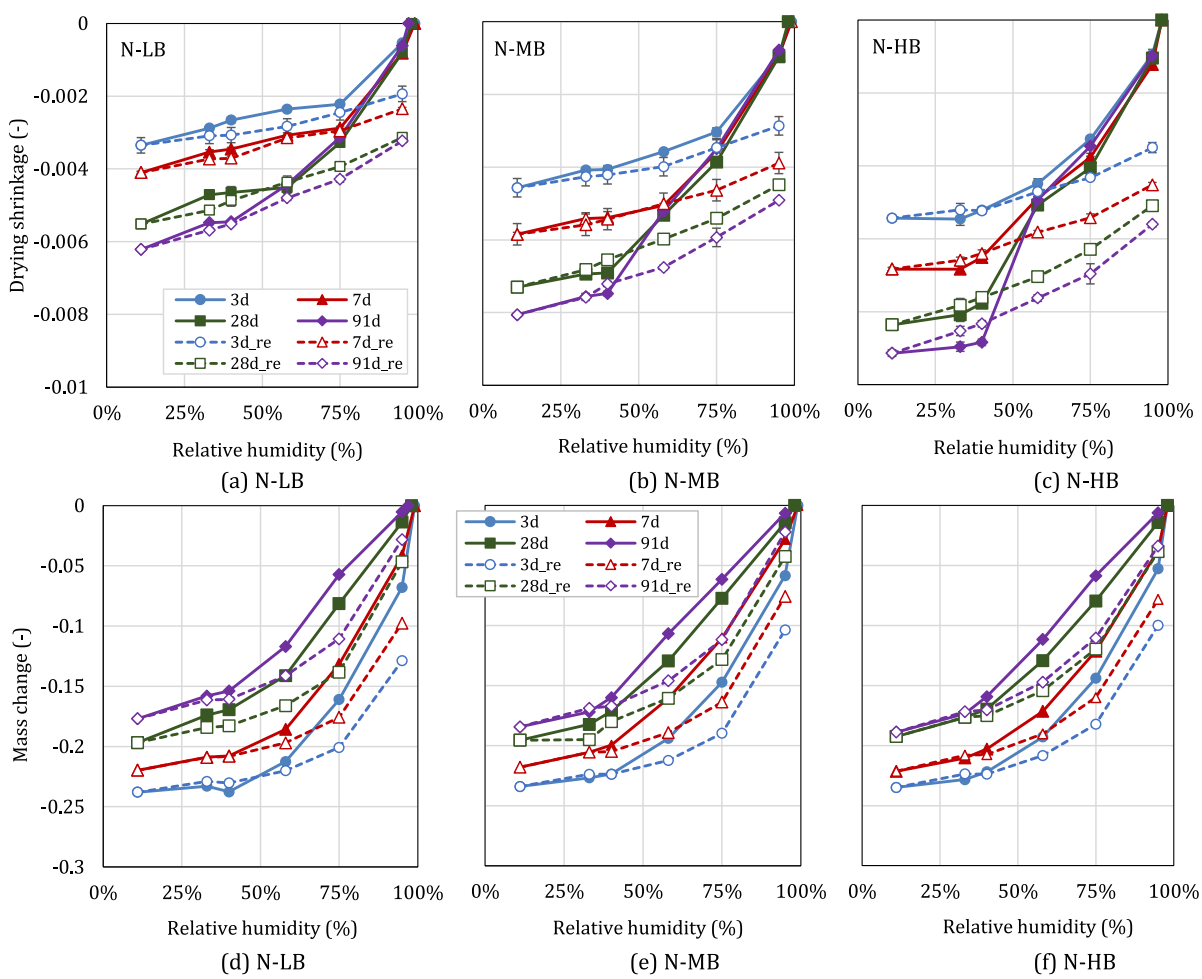

Fig. 5. Length change isotherms of (a) N-LB, (b) N-MB, and (c) N-HB and mass change isotherms of (d) N-LB, (e) N-MB, and (f) N-HB at start of drying at 3, 7, 28, and 91 d. Error bars represent standard deviation. Error bars for mass change isotherms are within the mark and omitted.

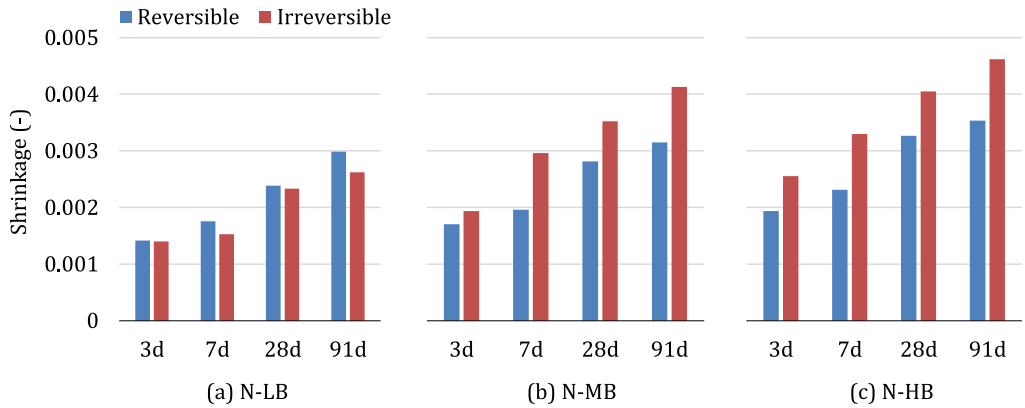

Fig. 6. Reversible strain (strain in rehumidifying branch from 11 % RH to 95 % RH) and irreversible strain (subtraction of reversible shrinkage from total drying shrinkage from 95 % RH to 11 % RH) of N-LB, N-MB, and N-HB.

data of QXRD.

The water vapor sorption isotherms were measured at 20 °C via the volumetric method using VSTAR (Quantachrome instrument). A sample (25 ± 5 mg) was used for each measurement at 20 °C, with a pressure tolerance of 0.05 mmHg and a time tolerance of 120 s. The adsorption and desorption branches were measured at intervals of $p/p_0 = 0.05$ up to 0.95, and ended at 0.98 (at 98 % RH). The BET [75] area (S_{H2O}) of the adsorption branch was calculated based on a water molecule cross-sectional area of 0.114 nm^2 [76–78]. The samples were ground in a ball mill, and sample powders with diameters of 25–75 μm were used to perform an analysis. For pretreatment, the samples were dried using a vacuum pump (theoretical minimum pressure of 6.7×10^{-2} Pa, observed maximum pressure of ~30 Pa) at room temperature for 4 h. The specimens at the start of drying and the specimens dried at 11 % RH for 1 year were used. Two measurements were performed for each condition.

The nitrogen sorption of the samples was measured using the same sample conditions as those for the water vapor isotherms at 77.4 K using a BELSORP mini II (MicrotracBEL Corp.). The S_{N2} of the adsorption branch was calculated using BET theory. The specimens were used at the start of the drying process. Two measurements were performed for each condition.

3. Results

3.1. Hydration degree at start of drying

The hydration degree of each mineral as well as the average values at the start of drying is summarized in Fig. 2. As shown, the hydration degree of the alite and aluminate phases (C_3A) at 3 d was higher because the cement was finer, whereas that of belite did not differ among the three hcps. Only N-MB and N-HB at 91 d indicated the same hydration degree; however, in general, the finer cement indicated a higher hydration degree at each age.

3.2. Microstructure development

The nitrogen sorption and water vapor sorption values measured in this study are summarized in Fig. 3. In the cases of N-LB and N-MB, the maximum sorption amount increased with the curing age. In the case of N-HB, the maximum sorption amount of nitrogen at 91 d was smaller than that at 28 d. This indicated that the outer C–S–H might be densified by the new precipitation of C–S–H in gel pores [79], and some of the mesopores created by the outer C–S–H could not be detected by the nitrogen molecules. By contrast, the water vapor sorption amount increased continuously with the curing age.

S_{N2} and S_{H2O} were plotted as a function of age, as shown in Fig. 4(a) and (b), respectively. As suggested by the maximum sorption amount, the S_{N2} of N-HB at 91 d decreased slightly from S_{N2} at 28 d. In fact, this trend was observed in a previous study [80] with a lower water-to-cement ratio.

The finer cement showed a higher S_{N2} at the same age. The higher S_{N2} was also confirmed based on the same hydration degree. By contrast, after 7 d, the S_{H2O} of N-MB and N-HB showed similar values. It is noteworthy that the S_{H2O} of N-LB at 91 d indicated the largest value, whereas that of N-LB indicated a cross-over against those of N-MB and N-HB. The S_{H2O} of the specimens dried under 11 % RH for 1 year ($S_{H2O,11\%RH}$) is shown in Fig. 4(b). As reported in previous publications, $S_{H2O,11\%RH}$ was smaller than S_{H2O} [49,81,82]. It reduced by approximately 20 % at 3 d and decreased gradually as hydration progressed, with a 37 % reduction for N-MB and N-HB and 48 % for N-LB at 91 d.

3.3. Length change and mass change isotherms

The length change and mass change isotherms are shown in Fig. 5. First, the drying shrinkage of the hcp increased with the hydration degree. This trend was confirmed in our previous study [83] and by other researchers [84]; however, the opposite trend, which was confirmed by specimens with a larger sectional area, was confirmed in concrete [71,85]. The coarser cement at an early age showed low RH hysteresis, and the rehumidifying branch at 33 % and 40 % RH showed slightly greater shrinkage than those in the first drying branch. For the matured and finer cement, different trends, i.e., the shrinkage at 33 % RH and 40 % RH in the first drying branch was greater than that in the desorption branch. In was previously reported that no hysteresis occurs below 40 % RH in general [37]. The reason is yet to be elucidated; however, assuming that the evaporable water in hcp is primarily entrapped by C–S–H sheets, i.e. gel pores and interlayer pores [86,87], and that unstable evaporable water is entrapped by C–S–H sheets whose entries are as narrow as C–S–H interlayer spaces [88], such an additional shrinkage is attributable to the capillary effect.

The mass change isotherms of N-LB, N-MB, and N-HB were comparable. The earlier the start of drying is, the greater mass loss is. And the mass at the 95 % RH in desorption and re-humidifying processes are different and its difference becomes larger as the start of drying is earlier.

The reversible shrinkage strain from 11 % RH to 95 % RH in the rehumidifying branch and irreversible strain at 95 % RH (differential strain at 95 % between the first drying branch and rehumidifying branch) of all the series are summarized in Fig. 6. The irreversible strain increased as the cement became hydrated, and the finer cement exhibited a larger irreversible strain. The reversible shrinkage exhibited

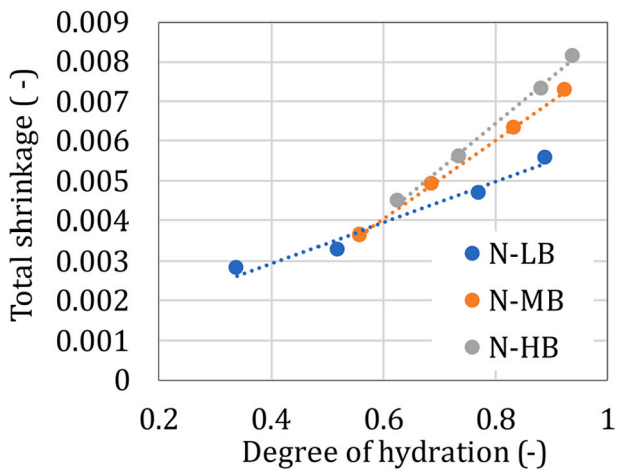

Fig. 7. Relationship between total shrinkage (drying shrinkage at 11 % RH) and degree of hydration.

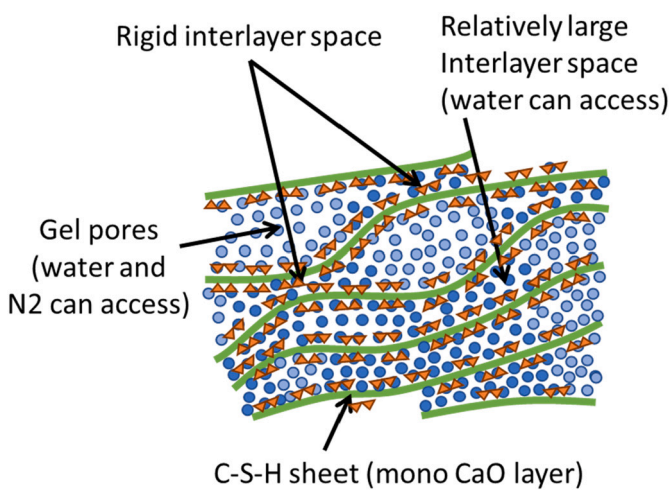

Fig. 8. Schematic figure of microstructure of C–S–H. Dark and light blue circles indicate water molecules, green line shows calcium oxide layer of C–S–H, and orange triangles represent silicate. The interlayer calcium ion is removed in this figure for clarity. (For interpretation of the references to color in this figure legend, the reader is referred to the web version of this article.)

similar trends.

4. Discussion

4.1. Effect of cement fineness on drying shrinkage

Fig. 7 depicts the relationship between the total drying shrinkage at 11 % RH of each hcp and the degree of hydration of hcp at the start of drying. After three days, each batch demonstrates a linear relationship between the total drying shrinkage and degree of hydration, but clearly, their lines do not overlap; in other words, the same degree of hydration does not correspond to the same total drying shrinkage, and finer cement exhibits a larger total drying shrinkage.

4.2. Effect of cement fineness on microstructure

First, the microstructure development is discussed. To evaluate the surface area of the hardened cement paste, the surface area per unit volume of hcp ($S_{N2,v}$ and $S_{H2O,v}$) as a function of the hydration degree (which are the data of "Cement" shown in Fig. 2) is shown in Fig. 9. $S_{N2,v}$ and $S_{H2O,v}$ were calculated using the QXRD results and the data shown in Fig. 4. Based on the QXRD results, each phase of the cement hydrates dried at 105 °C was calculated. In this process, C–S–H was assumed to be $C_{1.7}SH_{1.5}$ [42]. The $S_{N2,v}$ and $S_{N2,v}$ of N-HB were ~10 m^2/cm^3 higher than those of N-MB and N-LB, indicating that the finer cement produced a significant amount of low-density C–S–H. A similar trend was suggested by the data presented in ref. [66]. Meanwhile, the $S_{H2O,v}$ of N-HB and N-MB showed similar trends, as shown in Fig. 4, where that of N-HB was slightly lower than that of N-MB. These $S_{H2O,v}$ values of N-HB and N-MB were higher than that of N-LB in the hydration degree range of less than 0.8. However, beyond the hydration degree of 0.85, cross-over was observed and N-LB indicated the highest $S_{N2,v}$. These trends show that $S_{H2O,v}$ was affected by the fineness of cement at an early age (in the hydration degree range of less than 0.8), although the effect was insignificant.

To clarify these complicated phenomena, first, three different pores were assumed based on the studies of Brunauer et al. [78,89], namely, a rigid interlayer space, a relatively large interlayer space, and a gel space as shown in Fig. 8. To calculate the surface area of these spaces, 755 m^2/g of the C–S–H sheet was assumed [78,89]. Based on the amorphous phase detected by QXRD, the total amount of C–S–H and the resultant total C–S–H surface area were calculated. The surface area not detectable by water vapor or nitrogen was regarded as the surface area of the rigid interlayer space of C–S–H (surface area of fine interlayer space, $S_{F\text{-}int}$, which is calculated as S_{total} - S_{H2O}). According to Brunauer [90] and Odler [77], part of S_{H2O} is accessible by nitrogen molecules owing to differences in temperature conditions as well as the polarity of water molecules. Based on Tennis and Jennings [66], S_{N2} was regarded as the surface area of the gel space, in which a larger distance of C–S–H sheets was observed [44,64]. The surface area accessible only by water molecules was regarded as the surface area of the large interlayer space, $S_{L\text{-}int}$. The development of these spaces is shown as a function of the hydration degree in Fig. 10.

In general, the total surface area is determined by the amount of C–S–H, which can be approximated based on the hydration degree. At an early age, $S_{F\text{-}int}$ occupied approximately 70 % of the total C–S–H surface area, and the ratio of $S_{F\text{-}int}$ decreased gradually, as measured for the N-LB case. Finally, it became approximately 50 %, whereas $S_{L\text{-}int}$ was 29 % and S_{gel} was 21 %. For N-HB, the final compositions of $S_{F\text{-}int}$, $S_{L\text{-}int}$, and S_{gel} were 54 %, 20 %, and 26 %, respectively.

The ratio of $S_{F\text{-}int}$ decreased as the cement hydrated, whereas S_{gel} and $S_{L\text{-}int}$ increased. In the finer cement, S_{gel} increased, whereas $S_{F\text{-}int}$ decreased. This indicates that irregular spaces were created in the later stage of the hydration process; in fact, this occurred particularly when finer cement was used.

4.3. Reversible strain

A reversible strain occurred after an irreversible microstructure change under the first drying, and this strain is based on the amount of C–S–H in the hcp, as shown in Fig. 6. Based on this hypothesis, the reversible strain was plotted as a function of the hydration degree, as shown in Fig. 11. As shown, a clear correlation was confirmed. However, the trend exhibited a bilinear relationship, and the slopes above the hydration degree of 0.5 and below were different. This might be because the hydration degree was lessened by the reactions of the calcium aluminate phase and/or calcium alumina-ferrite phase. Therefore, the reversible strain was plotted as a function of the water vapor BET surface area per unit volume of hcp after drying under 11 % RH ($S_{H2O,v}$), as shown in Fig. 12, because the deformable part of C–S–H was assumed to be associated with the irregular pore in the stabilized C–S–H generated by long-term drying. Despite the one anomaly identified, a clear linear relationship was confirmed. Hence, it can be deduced that the irreversible strain originated from the water-accessible pores in C–S–H after stabilization due to long-term drying, and that it is not affected by the cement fineness.

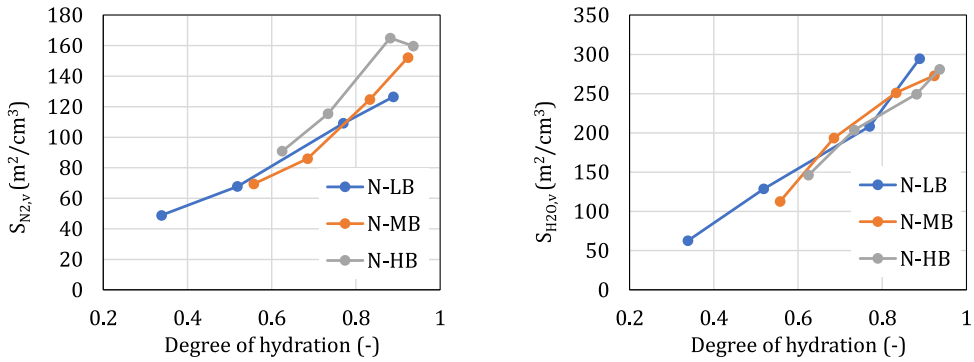

(a) S_{N2} (b) S_{H2O}

Fig. 9. (a) S_{N2} and (b) S_{H2O} of N-LB, N-MB, and N-HB as a function of hydration degree.

4.4. Total shrinkage and irreversible shrinkage

The results of the total shrinkage and irreversible shrinkage strain suggest that the microstructural changes under drying should be considered. S_{N2} changed significantly after drying [46,47,80], whereas S_{N2} did not correlate with the shrinkage strain. This suggests that the outer C–S–H or the low-density C–S–H, which increased when finer cement was used, did not contribute directly to the increase in the drying shrinkage.

Because the drying process is associated with water, $S_{H2O,v}$ was selected to confirm this relationship. Fig. 13 shows that the total strain and $S_{H2O,\ v}$ exhibits a linear relationship for each mixture, and that the finer cement is indicated by a greater slope. Because the drying shrinkage of hcp increases as the cement hydrates, the amount of C–S–H in the hcp is a key factor that affects the drying shrinkage. But this figure indicated that the quality of C–S–H from a view point of drying shrinkage is greatly affected by cement fineness.

After several trials, the best correlation was obtained based on an index of $S_{H2O,v} \times B$ (Blaine value, m^2/g). As shown in Fig. 14, the total shrinkage and irreversible strain exhibited a linear relationship with $S_{H2O,v} \times B$. This can be interpreted as follows:

Considering the similarity in geometry between the original grain boundary and reacted C–S–H precipitation, the final volume ratio of the outer C–S–H to the inner C–S–H in the hcp under the same water-to-cement ratio remains the same even when the cement fineness is changed (See Fig. 15(a), this is a scaleless image.). Therefore, the ratio of the outer C–S–H to the inner C–S–H will not contribute to the increase in the drying shrinkage. Assuming that the outer C–S–H and the inner C–S–H show isotropic shrinkage, there are two directions in which the shrinkage driving force propagates between C–S–H regions originating from different cement grains. One is vertical (V), shown in Fig. 15(a), and the other is horizontal (H), shown in Fig. 15(a). Force transmission in the direction (V) will not cause any difference in shrinkage when the cement fineness is changed because the force cannot be altered by the change in the surface area of cement. Consequently, the fineness of cement should change the force transmission in the direction (H). Assuming that the packing ratio of cement is constant, the final volume ratio of the outer C–S–H to the inner C–S–H is the same regardless of the cement fineness, so the distance between the original cement boundary should be changed. The increase in the surface area should decrease the space between original cement grain surfaces, as shown in Fig. 15(b). The outer C–S–H exhibited a fibrillar shape on the original grain boundary (e.g., Fig. 6 of [91]). Suppose the fibrillar outer C–S–H has the same order of diameter in any case. In that case, the length of C–S–H should be changed, and resultantly, the stiffness against horizontal force transmission (see Fig. 14(b)) of these fibrillar C–S–H beams is more significant than those whose cement fineness is low. In addition, this fibrillar shape of C–S–H will not be isotropic concerning the properties. There are CaO sheets of C–S–H along the direction of the fibril [91], Therefore, the basal space change of C–S–H occurs parallel to the circumferential direction (also parallel to the grain surface). The inner C–S–H is considered not to show irreversible shrinkage because when the water-to-cement ratio becomes lower, the irreversible shrinkage is reduced [39]. These phenomena can be represented by the following numerical expression:

$$\sigma_{eqsh} \propto \Delta\varepsilon_{interlayer} \bullet \left(\frac{S_{H2O}}{S_{total}}\right) \bullet V_{C-S-H} \bullet 2\left(\frac{3E_{fib}I_{fib}}{L_{fib}{}^{3}}\right) \Big/ B_v$$

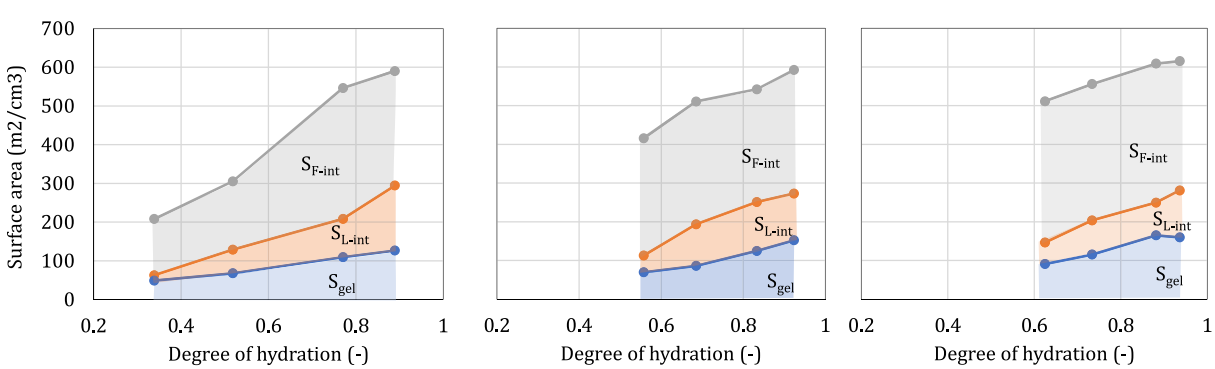

(a) N-LB (b) N-MB (c) N-HB

Fig. 10. Surface area development in N-LB (a), N-MB (b), and N-HB (c). S_{gel} is defined as surface area measured from nitrogen adsorption; $S_{L\text{-int}}$, surface area detected by water vapor sorption; $S_{F\text{-int}}$, surface area of C–S–H not detectable by either nitrogen or water vapor molecules.

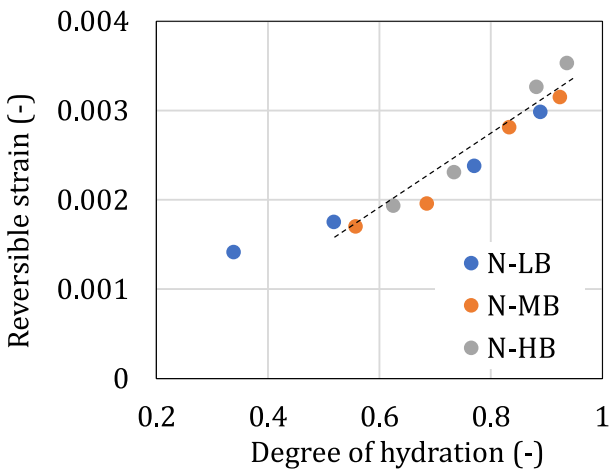

Fig. 11. Relationship between reversible strain and hydration degree of cement. Reversible strain is defined as incremental strain from 11 % RH to 95 % RH after specimen was dried under 11 % RH for 1 year. The dotted line is the result of liner fitting of the data except for one anomaly point.

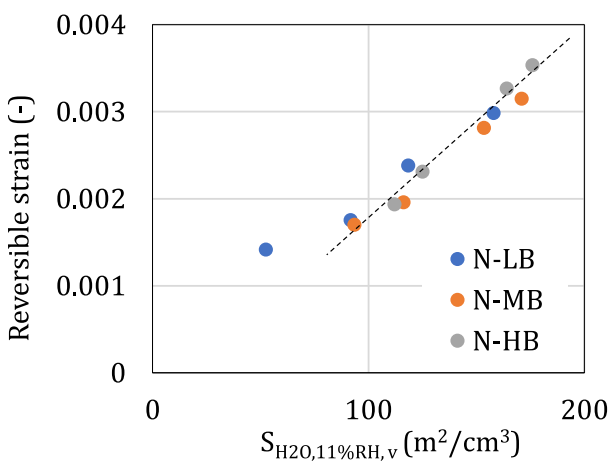

Fig. 12. Relationship between reversible strain and $S_{H2O,11\%RH,v}$, (water vapor BET surface area of hcp per unit volume of hcp after drying under 11 % RH for 1 year). The dotted line is the result of liner fitting of the data except for one anomaly point.

$$\propto \Delta\varepsilon_{interlayer} \bullet \left(\frac{S_{H2O}}{S_{total}}\right) \bullet V_{C-S-H}(S_{H2O}) \bullet 2\left(\frac{3E_{fib}I_{fib}}{w^3}\right)B_v^{\ n}$$

where σ_{eqsh}: equivalent driving stress of shrinkage of cement paste (N/m^2), $\Delta\varepsilon_{interlayer}$: volume change of C–S–H layers which can change their layer distance due to removal of water molecules (non-unit), $\left(\frac{S_{H2O}}{S_{total}}\right)$: a ratio of the spaces of C–S–H in which the layer distance can be changed by the removal of water molecules to the total surface area of C–S–H and this is the intrinsic value of C–S–H (non-unit), $V_{C-S-H}(S_{H2O})$: volume of C–S–H per volume of cement paste (m^3/m^3-paste) which can be represented by the S_{H2O} (m^2/m^3-paste), E_{fib}: Young's modulus of C–S–H fibril (N/m^2), I_{fib}: geometrical moment of inertia of fibril (m^4), L_{fib}: length of distance between original boundary cement grains (m) which can be represented by (w/B_v), w: volume of water in mixture proportion of the paste (m^3/m^3-paste) B_v: Blain of cement per unit volume of cement paste (m^2/m^3-paste).

Because S_{H2O} is a good indicator of the amount of C–S–H as shown in Fig. 9(b), V_{C-S-H} can be expressed by using a liner expression using S_{H2O}. The stiffness of the C–S–H fibril is a function of the length of the distance of original cement boundaries and specific nature of the C–S–H fibril. If we consider the simple beams, the stiffness of the beams is reciprocally proportional to the cube of the length of the distance between original cement boundaries. Each beam action should be normalized per the area where the beams grow up, corresponding to the original cement surface area. In this case, the shrinkage of cement paste can be represented by the factor of $S_{H2O} \times B^n$, where n is 2, while this is based on the perfect rectangular beam, n can be changed in the realistic case. Since this consideration is a very simplified one, further investigation is necessary.

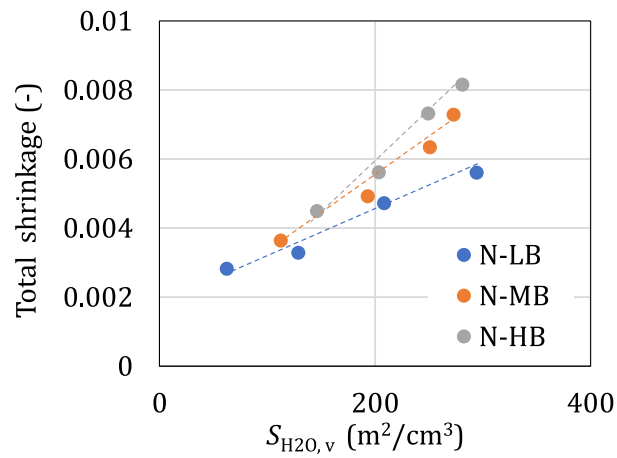

Fig. 13. Relationship between total shrinkage strain from 95 % RH to 11 % RH and $S_{H2O,v}$.

Based on these considerations, the shrinkage behavior of outer C–S–H, which shows the shrinkage in the circumferential direction, and change in the length of outer C–S–H or distance between the original cement grain surfaces due to cement fineness is the critical factor in the increase in shrinkage of hcp.

From a viewpoint of engineering application, the large drying shrinkage of the hardened cement paste should lead to large drying shrinkage of concrete, although their quantitative relationship has not yet been fully clarified [92–94], especially the impact of cracking around the aggregates, the additional hydration process of cement at the inner part of the specimen, and mutual stress interaction between periphery concrete and central concrete seemed significant but they are not appropriately considered. If a concrete member is subjected to external restraint, drying shrinkage-induced cracks occur. This crack opening process has a significant impact on the durability of the reinforced concrete member, as discussed in the Introduction section, as well as the stiffness change and possible loading capacity change of the reinforced concrete member (for example, [25,27]). In addition, the microcracks around the aggregates cause a decrease in the Young's modulus of concrete [9,95]. The rapid construction process of reinforced concrete structures using finer cement may reduce the durability and change the long-term mechanical performance. Thus, it is strongly suggested to qualitatively evaluate this trade-off relationship.

5. Conclusion

The effect of the fineness value of cement on the drying shrinkage behavior was investigated. Shrinkage and mass change isotherms of cement paste with three different cement fineness values were obtained for four different curing ages. The degree of hydration, water vapor sorption, and nitrogen adsorption isotherms were obtained at different ages at the start of drying. The following conclusions were obtained based on experimental investigations:

1) The degree of hydration and drying shrinkage strain demonstrated a linear relationship for each batch. However, these relationships were

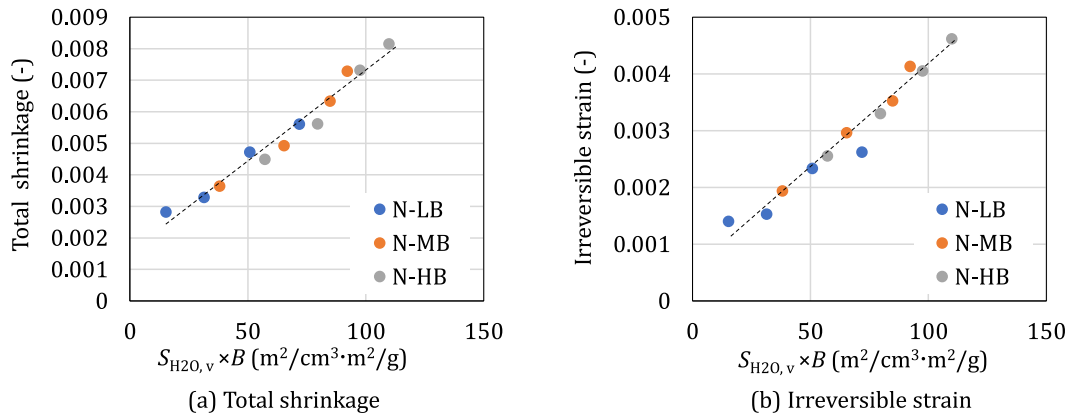

Fig. 14. Relationships between (a) total shrinkage and $S_{H2O,v} \times$ B and (b) irreversible strain and $S_{H2O,v} \times$ B.

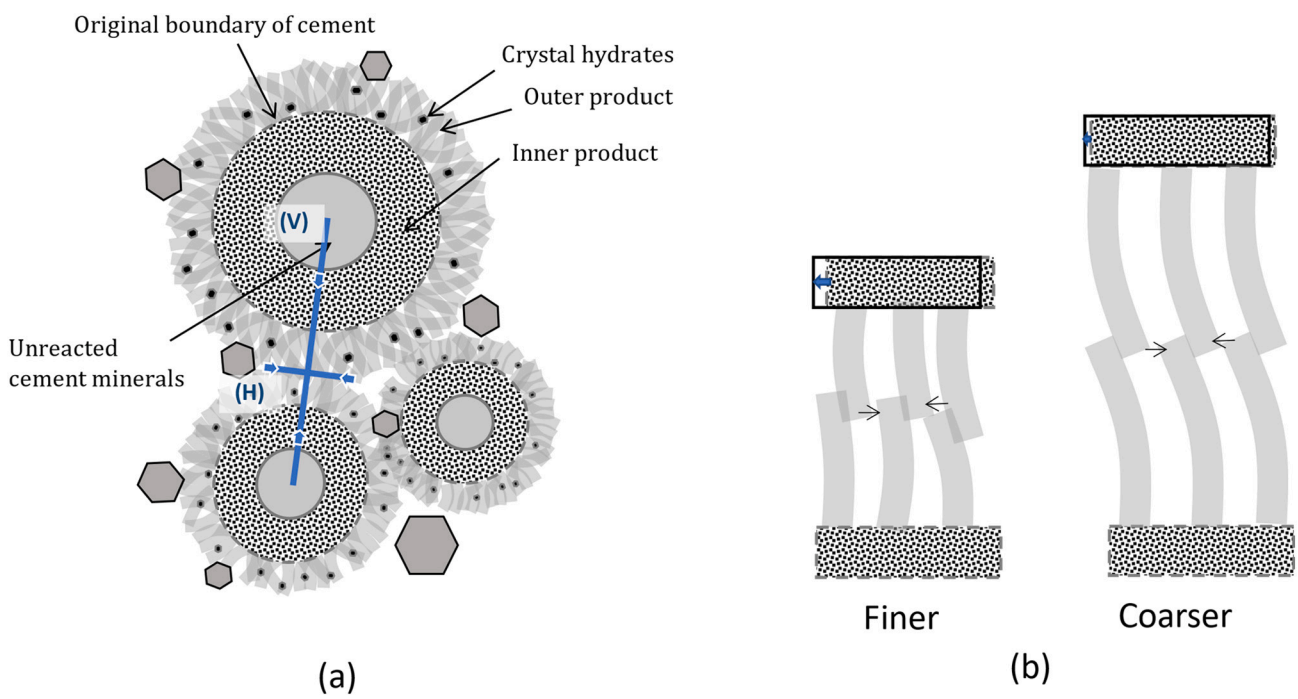

Fig. 15. (a) Schematic microstructure of hardened cement paste. The driving force of shrinkage in the direction (V) will not cause the difference in the shrinkage of hcp by changing the cement fineness. Only the driving force of shrinkage in the direction (H) changes the shrinkage of hcp by changing the cement fineness. (b) Assuming the same diameter of fibrillar C–S–H on the top of inner C–S–H, horizontal shrinkage driving force is well transmitted between C–S–H structures when the distance is shorter.

not identical. Therefore, the increase in the drying shrinkage of cement paste with finer cement cannot be solely explained by the faster degree of hydration, and other mechanisms should also be considered.

2) Drying shrinkage and irreversible shrinkage increased with the cement fineness. Therefore, an increase in the Blaine value or surface area of cement degrades the volume stability of the cement paste.
3) Reversible shrinkage was well predicted by the water vapor surface BET area of hcp dried under 11 % RH for a long period.
4) Drying shrinkage exhibited a linear relationship with the water vapor BET surface area of hcp at the start of drying for each mixture. However, the relationship changed when the cement fineness value was changed.
5) The total drying shrinkage and irreversible shrinkage were well predicted based on the index $S_{H2O,v} \times$ B, where B is the Blaine value of cement, and $S_{H2O,v}$ is the water vapor BET surface area of hcp.

CRediT authorship contribution statement

IM: Project administration, Supervision, Conceptualization, Methodology, Funding acquisition, Visualization, Writing - Original Draft, Writing – review & editing

HS: Methodology, Investigation, Data Curation, Visualization, Writing – review & editing

SU: Investigation, Methodology, Visualization, Writing – review & editing

RK: Investigation, Methodology, Visualization, Writing – review & editing

Declaration of competing interest

The authors declare that they have no known competing financial interests or personal relationships that could have appeared to influence the work reported in this paper.

Data availability

Data will be made available on request.

Acknowledgements

This study was partially funded by JSPS KAKENHI 18H03804, 19H00791, and collaboration research with Chubu Electric Company Co., Inc.

Appendix A

Regarding the cement fineness, nitrogen sorption, image analyzer, and laser diffraction method were applied. The same procedure as that for hardened cement paste described in the main text was applied for nitrogen sorption. The laser diffraction spectrometry (MT3300EXII, Microtrac BEL) was used by the wet method, in which cement particles were dispersed into isopropanol with sonication. The measurement duration was 50 s (10-s × five-time repetitions). Refractive indexes for solvent and cement were 1.38, and 1.71 (calculated from Table 3 of the main text), respectively. The results are summarized in Table. A1 and the linear relationships were confirmed.

Table A1
The surface area of cements detected by different methods.

	Blaine	N_2	Image analyzer	Laser diffraction
	cm^2/g	cm^2/g	cm^2/g	cm^2/g
N-LB	2440	8041	7691	48,691
N-MB	3380	9940	12,732	73,641
N-HB	3910	13,466	16,323	80,166

References

[1] R.W. Carlson, Drying shrinkage of concrete as affected by many factors, Am. Soc. Test. Mater. Proc. 38 (1938) 419–437.
[2] G. Pickett, Effect of aggregate on shrinkage of concrete and a hypothesis concerning shrinkage, ACI J. Proc. 52 (1956) 581–590, https://doi.org/10.14359/11617.
[3] T.C. Hansen, K.E.C. Nielsen, Influence of aggregate properties on concrete shrinkage, ACI J. 62 (1965) 783–794, https://doi.org/10.14359/7723.
[4] R.W. Carlson, T.J. Reading, Model study of shrinkage cracking in concrete building walls, ACI Struct. J. 85 (1988) 395–404, https://doi.org/10.14359/2666.
[5] J. Bisschop, J.G. van Mier, Effect of aggregates on drying shrinkage microcracking in cement-based composites, Mater. Struct. Constr. 35 (2002) 453–461, https://doi.org/10.1007/BF02483132.
[6] A. Idiart, J. Bisschop, A. Caballero, P. Lura, A numerical and experimental study of aggregate-induced shrinkage cracking in cementitious composites, Cem. Concr. Res. 42 (2012) 272–281, https://doi.org/10.1016/j.cemconres.2011.09.013.
[7] I. Maruyama, H. Sasano, Strain and crack distribution in concrete during drying, Mater. Struct. Constr. 47 (2014) 517–532, https://doi.org/10.1617/s11527-013-0076-7.
[8] I. Maruyama, A. Sugie, Numerical study on drying shrinkage of concrete affected by aggregate size, J. Adv. Concr. Technol. 12 (2014) 279–288, https://doi.org/10.3151/jact.12.279.
[9] I. Maruyama, H. Sasano, Y. Nishioka, G. Igarashi, Strength and Young's modulus change in concrete due to long-term drying and heating up to 90 °C, Cem. Concr. Res. 66 (2014) 48–63, https://doi.org/10.1016/j.cemconres.2014.07.016.
[10] H. Sasano, I. Maruyama, Mechanism of drying-induced change in the physical properties of concrete: a mesoscale simulation study, Cem. Concr. Res. 143 (2021), 106401, https://doi.org/10.1016/J.CEMCONRES.2021.106401.
[11] I. Yurtdas, N. Burlion, F. Skoczylas, Triaxial mechanical behaviour of mortar: effects of drying, Cem. Concr. Res. 34 (2004) 1131–1143, https://doi.org/10.1016/j.cemconres.2003.12.004.
[12] K. Kishitani, H. Kasami, F. Oshida, R. Okuno, in: Property of Concrete Exposed to Sustained Elevated Temperature Ranging 20 to 300 °C: Part 1,2, Summ. Tech. Pap. AIJ Annu. Meet, 1982, pp. 317–320.
[13] N. Burlion, F. Bourgeois, J.-F. Shao, Effects of desiccation on mechanical behaviour of concrete, Cem. Concr. Compos. 27 (2005) 367–379, https://doi.org/10.1016/j.cemconcomp.2004.05.004.
[14] S.E. Pihlajavaara, A review of some of the main results of a research on the ageing phenomena of concrete: effect of moisture conditions on strength, shrinkage and creep of mature concrete, Cem. Concr. Res. 4 (1974) 761–771, https://doi.org/10.1016/0008-8846(74)90048-9.
[15] M. Lin, M. Itoh, I. Maruyama, L. Mao, I. Mitsuki, M. Ippei, Mechanism of change in splitting tensile strength of concrete during heating or drying up to 90°C, J. Adv. Concr. Technol. 13 (2015) 94–102, https://doi.org/10.3151/jact.13.94.
[16] J.A. Hanson, Effects of curing and drying enviroments on splitting tensile strength of concrete, J. Proc. 65 (1968), https://doi.org/10.14359/7495.
[17] S. Popovics, Effect of curing method and final moisture condition on compressive strength of concrete, J. Am. Concr. Inst. 83 (1986) 650–657, https://doi.org/10.14359/10658.
[18] D. Naus, A Compilation of Elevated Temperature Concrete Material Property Data and Information for Use in Assessments of Nuclear Power Plant Reinforced Concrete Structures 328, 2010 doi:NUREG/CR-7031.
[19] F.H. Wittmann, Interaction of hardened cement paste and water, J. Am. Ceram. Soc. 56 (1973) 409–415, https://doi.org/10.1111/j.1151-2916.1973.tb12711.x.
[20] P.J. Sereda, R.F. Feldman, E.G. Swenson, Effect of sorbed water on some mechanical properties of hydrated Portland cement paste and compacts, Highw. Res. Board Spec. Rep. (1966) 58–73.
[21] I. Yurtdas, N. Burlion, F. Skoczylas, Experimental characterisation of the drying effect on uniaxial mechanical behaviour of mortar, Mater. Struct. 37 (2004) 170–176, https://doi.org/10.1007/bf02481616.
[22] I. Maruyama, G. Igarashi, Cement reaction and resultant physical properties of cement paste, J. Adv. Concr. Technol. 12 (2014) 200–213, https://doi.org/10.3151/jact.12.200.
[23] Y. Yao, L. Wang, F.H. Wittmann, Publications on durability of reinforced concrete structures under combined mechanical loads and environmental actions: An annotated bibliography, Aedificatio Publishers, 2013.
[24] I. Maruyama, Multi-scale review for possible mechanisms of natural frequency change of reinforced concrete structures under an ordinary drying condition, J. Adv. Concr. Technol. 14 (2016) 691–705, https://doi.org/10.3151/jact.14.691.
[25] H. Sasano, I. Maruyama, A. Nakamura, Y. Yamamoto, M. Teshigawara, Impact of drying on structural performance of reinforced concrete shear walls, J. Adv. Concr. Technol. 16 (2018) 210–232, https://doi.org/10.3151/jact.16.210.
[26] R. Kurihara, N. Chijiwa, K. Maekawa, Thermo-hygral analysis on long-term natural frequency of RC buildings with different dimensions, J. Adv. Concr. Technol. 15 (2017) 381–396, https://doi.org/10.3151/jact.15.381.
[27] P. Satya, T. Asai, M. Teshigawara, Y. Hibino, I. Maruyama, Impact of drying on structural performance of reinforced concrete beam with slab, Materials (Basel). 14 (2021) 1887, https://doi.org/10.3390/ma14081887.
[28] K. Nakarai, S. Morito, M. Ehara, S. Matsushita, Shear strength of reinforced concrete beams: concrete volumetric change effects, J. Adv. Concr. Technol. 14 (2016) 229–244, https://doi.org/10.3151/jact.14.229.
[29] C. Jaafari, D. Bertrand, T. Guillot, E. Prudhomme, N. Tardif, J.F. Georgin, F. Delhomme, R. Trunfio, N. Chateur, E. Bruyere, E. Augeard, L. Baillet, P. Guéguen, S. Grange, Effect of early age drying shrinkage on the seismic response of RC structures, Mater. Struct. Constr. 53 (2020) 1–19, https://doi.org/10.1617/s11527-020-01552-2.
[30] T.C. Powers, The mechanics of shrinkage and reversible creep of hardened cement paste, Int. Conf. Struct. Concr. (1965) 319–344.
[31] R.F. Feldman, P.J. Sereda, A model for hydrated Portland cement paste as deduced from sorption-length change and mechanical properties, Matériaux Constr. 1 (1968) 509–520, https://doi.org/10.1007/BF02473639.
[32] F.H. Wittmann, Surface tension skrinkage and strength of hardened cement paste, Matériaux Constr. 1 (1968) 547–552, https://doi.org/10.1007/BF02473643.
[33] Z.P. Bažant, Thermodynamics of hindered adsorption and its implications for hardened cement paste and concrete, Cem. Concr. Res. 2 (1972) 1–16, https://doi.org/10.1016/0008-8846(72)90019-1.
[34] A. Bentur, R.L. Berger, F.V. Lawrence, N.B. Milestone, S. Mindess, J.F. Young, Creep and drying shrinkage of calcium silicate pastes III. A hypothesis of irreversible strains, Cem. Concr. Res. 9 (1979) 83–95, https://doi.org/10.1016/0008-8846(79)90098-X.

[35] W. Hansen, Drying shrinkage mechanisms in Portland cement paste, J. Am. Ceram. Soc. 70 (1987) 323–328, https://doi.org/10.1111/j.1151-2916.1987.tb05002.x.
[36] F. Beltzung, F.H. Wittmann, Role of disjoining pressure in cement based materials, Cem. Concr. Res. 35 (2005) 2364–2370, https://doi.org/10.1016/j.cemconres.2005.04.004.
[37] I. Maruyama, Origin of drying shrinkage of hardened cement paste: hydration pressure, J. Adv. Concr. Technol. 8 (2010) 187–200, https://doi.org/10.3151/jact.8.187.
[38] G. El Tabbal, P. Dangla, M. Vandamme, M. Bottoni, S. Granet, Modelling the drying shrinkage of porous materials by considering both capillary and adsorption effects, J. Mech. Phys. Solids. 142 (2020), 104016, https://doi.org/10.1016/j.jmps.2020.104016.
[39] R.A. Helmuth, D.M.H. Turk, The reversible and irreversible drying shrinkage of hardened Portland cement and tricalcium silicate paste, Portl. Cem. Assoc. J. Res. Dev. Lab. 9 (1967) 8–21.
[40] L. Jesser, Kolloide chemische reaktionen des tonerdezementmörtels, Zement. 16 (1927) 741.
[41] H.M. Jennings, A model for the microstructure of calcium silicate hydrate in cement paste, Cem. Concr. Res. 30 (2000) 101–116, https://doi.org/10.1016/S0008-8846(99)00209-4.
[42] H.M. Jennings, Refinements to colloid model of C-S-H in cement: CM-II, Cem. Concr. Res. 38 (2008) 275–289, https://doi.org/10.1016/j.cemconres.2007.10.006.
[43] M. Abuhaikal, K. Ioannidou, T. Petersen, R.J.-M. Pellenq, F.J. Ulm, Le Châtelier's conjecture: measurement of colloidal eigenstresses in chemically reactive materials, J. Mech. Phys. Solids. 112 (2018) 334–344, https://doi.org/10.1016/j.jmps.2017.12.012.
[44] I. Maruyama, T. Ohkubo, T. Haji, R. Kurihara, Dynamic microstructural evolution of hardened cement paste during first drying monitored by 1H NMR relaxometry, Cem. Concr. Res. 122 (2019) 107–117, https://doi.org/10.1016/j.cemconres.2019.04.017.
[45] I. Maruyama, G. Igarashi, Y. Nishioka, Bimodal behavior of C-S-H interpreted from short-term length change and water vapor sorption isotherms of hardened cement paste, Cem. Concr. Res. 73 (2015) 158–168, https://doi.org/10.1016/j.cemconres.2015.03.010.
[46] G.G. Litvan, R.E. Myers, Surface area of cement paste conditioned at various relative humidities, Cem. Concr. Res. 13 (1983) 49–60, https://doi.org/10.1016/0008-8846(83)90127-8.
[47] L.J. Parrott, W. Hansen, R.L. Berger, Effect of first drying upon the pore structure of hydrated alite paste, Cem. Concr. Res. 10 (1980) 647–655, https://doi.org/10.1016/0008-8846(80)90028-9.
[48] A. Bogner, J. Schatz, F. Dehn, H.S. Müller, Influence of drying on the microstructure of hardened cement paste: a mercury intrusion porosimetry, nitrogen sorption and SAXS study, J. Adv. Concr. Technol. 18 (2020) 83–94, https://doi.org/10.3151/jact.18.83.
[49] I. Maruyama, Y. Nishioka, G. Igarashi, K. Matsui, Microstructural and bulk property changes in hardened cement paste during the first drying process, Cem. Concr. Res. 58 (2014) 20–34, https://doi.org/10.1016/j.cemconres.2014.01.007.
[50] J. Kropp, T. Gräfenecker, H.K. Hilsdorf, Characterization of the microstructure of hydrated cement paste by small angle X-ray scattering, in: J.W. Arrowsmith (Ed.), En Princ, Appl. Pore Struct. Charact, Bristol, 1985, pp. 83–96.
[51] J.J. Völkl, R.E. Beddoe, M.J. Setzer, The specific surface of hardened cement paste by small-angle X-ray scattering effect of moisture content and chlorides, Cem. Concr. Res. 17 (1987) 81–88, https://doi.org/10.1016/0008-8846(87)90062-7.
[52] W.S. Chiang, E. Fratini, P. Baglioni, D. Liu, S.H. Chen, Microstructure determination of calcium-silicate-hydrate globules by small-angle neutron scattering, J. Phys. Chem. C 116 (2012) 5055–5061, https://doi.org/10.1021/jp300745g.
[53] J.J. Thomas, A.J. Allen, H.M. Jennings, Structural changes to the calcium-silicate-hydrate gel phase of hydrated cement with age, drying, and resaturation, J. Am. Ceram. Soc. 91 (2008) 3362–3369, https://doi.org/10.1111/j.1551-2916.2008.02636.x.
[54] I. Maruyama, N. Sakamoto, K. Matsui, G. Igarashi, Microstructural changes in white Portland cement paste under the first drying process evaluated by WAXS, SAXS, and USAXS, Cem. Concr. Res. 91 (2016) 24–32, https://doi.org/10.1016/j.cemconres.2016.10.002.
[55] I. Maruyama, G. Igarashi, K. Matsui, N. Sakamoto, Hinderance of C-S-H sheet piling during first drying using a shrinkage reducing agent: a SAXS study, Cem. Concr. Res. 144 (2021), 106429, https://doi.org/10.1016/j.cemconres.2021.106429.
[56] P.C. Fonseca, H.M. Jennings, The effect of drying on early-age morphology of C-S-H as observed in environmental SEM, Cem. Concr. Res. 40 (2010) 1673–1680, https://doi.org/10.1016/j.cemconres.2010.08.007.
[57] W. Soja, F. Georget, H. Maraghechi, K. Scrivener, Evolution of microstructural changes in cement paste during environmental drying, Cem. Concr. Res. 134 (2020), 106093, https://doi.org/10.1016/j.cemconres.2020.106093.
[58] D.H. Bager, E.J. Sellevold, Ice formation in hardened cement paste, part II - drying and resaturation on room temperature cured pastes, Cem. Concr. Res. 16 (1986) 835–844, https://doi.org/10.1016/0008-8846(86)90006-2.
[59] R.E. Beddoe, M.J. Setzer, A low-temperature DSC investigation of hardened cement paste subjected to chloride action, Cem. Concr. Res. 18 (1988) 249–256, https://doi.org/10.1016/0008-8846(88)90009-9.
[60] X. Cong, R.J. Kirkpatrick, Effects of the temperature and relative humidity on the structure of C-S-H gel, Cem. Concr. Res. 25 (1995) 1237–1245, https://doi.org/10.1016/0008-8846(95)00116-T.
[61] A. Gajewicz, Characterisation of Cement Microstructure and Pore – Water Interaction by 1H Nuclear Magnetic Resonance Relaxometry, 2014.
[62] A.C.A. Muller, K.L. Scrivener, A.M. Gajewicz, P.J. McDonald, Use of bench-top NMR to measure the density, composition and desorption isotherm of C-S-H in cement paste, Microporous Mesoporous Mater. 178 (2013) 99–103, https://doi.org/10.1016/j.micromeso.2013.01.032.
[63] I. Maruyama, T. Ohkubo, T. Haji, R. Kurihara, Reply to zhou et al'.S "A discussion of the paper 'Dynamic microstructural evaluation of hardened cement paste during first drying monitored by 1H NMR relaxometry'", Cem. Concr. Res. 137 (2020), 106219 https://doi.org/10.1016/J.CEMCONRES.2020.106219.
[64] I.G. Richardson, Nature of C-S-H in hardened cements, Cem. Concr. Res. 29 (1999) 1131–1147, https://doi.org/10.1016/S0008-8846(99)00168-4.
[65] J.J. Thomas, H.M. Jennings, A.J. Allen, The surface area of cement paste as measured by neutron scattering: evidence for two C-S-H morphologies, Cem. Concr. Res. 28 (1998) 897–905, https://doi.org/10.1016/S0008-8846(98)00049-0.
[66] P.D. Tennis, H.M. Jennings, A model for two types of calcium silicate hydrate in the microstructure of Portland cement pastes, Cem. Concr. Res. 30 (2000) 855–863, https://doi.org/10.1016/S0008-8846(00)00257-X.
[67] J.H. Taplin, A method for following the hydration reaction in Portland cement paste, Aust. J. Appl. Sci. 10 (1959) 329–345.
[68] S. Goto, M. Daimon, G. Hosaka, R. Kondo, Composition and morphology of hydrated tricalcium silicate, J. Am. Ceram. Soc. 59 (1976) 281–284, https://doi.org/10.1111/j.1151-2916.1976.tb10965.x.
[69] K.L. Scrivener, H.H. Patel, P.L. Pratt, L.J. Parrott, Analysis of phases in cement paste using backscattered electron images, methanol adsorption and thermogravimetric analysis, MRS Proc. 85 (1986), https://doi.org/10.1557/proc-85-67.
[70] A.C.A. Muller, K.L. Scrivener, A.M. Gajewicz, P.J. Mcdonald, Densification of C−S−H measured by 1H NMR relaxometry, J. Phys. Chem. C 403–412 (2013).
[71] E.W. Bennett, D.R. Loat, Shrinkage and creep of concrete as affected by the fineness of Portland cement, Mag. Concr. Res. 22 (1970) 69–78, https://doi.org/10.1680/macr.1970.22.71.69.
[72] D.P. Bentz, G. Sant, J. Weiss, Early-age properties of cement-based materials. I: influence of cement fineness, J. Mater. Civ. Eng. 20 (2008) 502–508, https://doi.org/10.1061/(ASCE)0899-1561(2008)20:7(502).
[73] H. Rahoui, I. Maruyama, M. Vandamme, J.-M. Pereira, M. Mosquet, Impact of an SRA (hexylene glycol) on irreversible drying shrinkage and pore solution properties of cement pastes, Cem. Concr. Res. 143 (2021), 106227, https://doi.org/10.1016/j.cemconres.2020.106227.
[74] R. Kurihara, I. Maruyama, Effects of heating and drying on the strength and stiffness of high-early-strength Portland cement pastes, Cem. Concr. Compos. 106 (2020), 103455, https://doi.org/10.1016/j.cemconcomp.2019.103455.
[75] S. Brunauer, P.H. Emmett, E. Teller, Adsorption of gases in multimolecular layers, J. Am. Chem. Soc. 60 (1938) 309–319, https://doi.org/10.1021/ja01269a023.
[76] R.S. Mikhail, L. Copeland, S. Brunauer, Pore structures and surface areas of hardened Portland cement pastes by nitrogen adsorption, Can. J. Chem. 42 (1964) 426–438.
[77] I. Odler, The BET-specific surface area of hydrated Portland cement and related materials, Cem. Concr. Res. 33 (2003) 2049–2056, https://doi.org/10.1016/S0008-8846(03)00225-4.
[78] S. Brunauer, D.L. Kantro, L.E. Copeland, The stoichiometry of the hydration of β-dicalcium silicate and tricalcium silicate at room temperature, J. Am. Chem. Soc. 80 (1958) 761–767, https://doi.org/10.1021/ja01537a001.
[79] A.C.A. Muller, K.L. Scrivener, A.M. Gajewicz, P.J. McDonald, Densification of C-S–H measured by 1H NMR relaxometry, J. Phys. Chem. C 117 (2013) 403–412, https://doi.org/10.1021/jp3102964.
[80] C.M. Hunt, Nitrogen sorption measurements and surface areas of hardened cement paste, Highw. Res. Broad Spec. Rep. 90 (1966) 112–122.
[81] L.A. Tomes, C.M. Hunt, R.L. Blaine, Some factors affecting the surface area of hydrated Portland cement as determined by water-vapor and nitrogen adsorption, J. Res. Natl. Bur. Stand. 59 (1957) (1934) 357, https://doi.org/10.6028/jres.059.039.
[82] C.M. Hunt, L.A. Tomes, R.L. Blaine, Some effects of aging on the surface area of Portland cement paste, J. Res. Natl. Bur. Stand. Sect. A Phys. Chem. 64A (1960) 163, https://doi.org/10.6028/jres.064a.016.
[83] T. Haji, S. Kotera, R. Kurihara, I. Maruyama, Impact of demolding age and mineral composition of cement on drying shrinkage of cement paste, Proc. Japan Concr. Inst. 38 (2016) 45–50.
[84] S. Nagamatsu, Y. Sato, Y. Ohtsune, Relationship between degree of drying and drying shrinkage strain of hardened cement paste (in Japanese), J. Struct. Constr. Eng. (1992) 13–21. http://ci.nii.ac.jp/naid/110004089847/en/.
[85] Aci, 209 committee., ACI 209R–92 prediction of creep, shrinkage, and temperature effects in concrete structures, American Concrete Institute (2009), https://doi.org/10.1201/9780203882955.ch168.
[86] P.J. McDonald, J. Mitchell, M. Mulheron, P.S. Aptaker, J.P. Korb, L. Monteilhet, Two-dimensional correlation relaxometry studies of cement pastes performed using a new one-sided NMR magnet, Cem. Concr. Res. 37 (2007) 303–309, https://doi.org/10.1016/j.cemconres.2006.01.013.
[87] L. Monteilhet, J.-P. Korb, J. Mitchell, P.J. McDonald, Observation of exchange of micropore water in cement pastes by two-dimensional T2–T2 nuclear magnetic resonance relaxometry nuclear magnetic resonance relaxometry, Phys. Rev. E 74 (2006), 061404, https://doi.org/10.1103/PhysRevE.74.061404.
[88] I. Maruyama, J. Rymeš, M. Vandamme, B. Coasne, Cavitation of water in hardened cement paste under short-term desorption measurements, Mater. Struct. Constr. 51 (2018), https://doi.org/10.1617/s11527-018-1285-x.
[89] S. Brunauer, D.L. Kantro, C.H. Weise, The surface energy of tobermorite, Can. J. Chem. 37 (1959) 714–724.

[90] S. Brunauer, I. Odler, M. Yudenfreund, The new model of hardened Portland cement paste, Highw. Res. Rec. (1970) 89–101.
[91] I.G.G. Richardson, Tobermorite/jennite- and tobermorite/calcium hydroxide-based models for the structure of C-S-H: applicability to hardened pastes of tricalcium silicate, β-dicalcium silicate, Portland cement, and blends of Portland cement with blast-furnace slag, metakaol, Cem. Concr. Res. 34 (2004) 1733–1777, https://doi.org/10.1016/j.cemconres.2004.05.034.
[92] F.De Larrard, R.Le Roy, The Influence of Mix Composition on Mechanical Properties of High-performance Silica-fume Concrete, Am. Concr. Institute, ACI Spec. Publ., 1992. SP132.
[93] B. Bissonnette, P. Pierre, M. Pigeon, Influence of key parameters on drying shrinkage of cementitious materials, Cem. Concr. Res. 29 (1999) 1655–1662, https://doi.org/10.1016/S0008-8846(99)00156-8.
[94] E. Rozière, S. Granger, P. Turcry, A. Loukili, Influence of paste volume on shrinkage cracking and fracture properties of self-compacting concrete, Cem. Concr. Compos. 29 (2007) 626–636, https://doi.org/10.1016/J.CEMCONCOMP.2007.03.010.
[95] I. Yurtdas, H. Peng, N. Burlion, F. Skoczylas, Influences of water by cement ratio on mechanical properties of mortars submitted to drying, Cem. Concr. Res. 36 (2006) 1286–1293, https://doi.org/10.1016/J.CEMCONRES.2005.12.015.